Biogeochemistry (2013) 112:389–407
DOI 10.1007/s10533-012-9734-z

Drought impacts on biogeochemistry and microbial processes in salt marsh sediments: a flow-through reactor approach

Laura Palomo · Christof Meile · Samantha B. Joye

Received: 6 February 2011 / Accepted: 23 March 2012 / Published online: 20 April 2012

Abstract The effects of drought on salt marsh sediments from Sapelo Island, Georgia, were examined in flow-through reactor experiments. Three hydrological treatments were employed: a continuously flooded anoxic control, a periodic drought treatment that experienced alternate periods of flooding and drying, and a severe drought treatment, where sediment was exposed to drought (drying) for several weeks and then flooded; the effect of both buffered and non-buffered flooding solutions were examined. In permanently anoxic sediments as well as in sediments exposed to drought, organic carbon oxidation was dominated by SO_4^{2-} reduction (SR) and SR rates increased over time. The shift from anoxic to oxic conditions in drought treatments significantly altered sediment geochemistry and pathways of microbial metabolism. Drought conditions favored suboxic mineralization processes, such as Fe(III) reduction and denitrification, which was fueled by NH_4^+ oxidation promoted by O_2 delivered during drought conditions. Other major drought-induced changes included pH decrease, and altered concentrations of solid phase adsorbed metals.

Keywords Drought · Salt marsh · Organic matter mineralization · Dieback

L. Palomo · C. Meile · S. B. Joye (✉)
Department of Marine Sciences, University of Georgia, Athens, GA 30602, USA
e-mail: mjoye@uga.edu

Introduction

Climate change will affect ecosystems through continued increases in temperature and changes in rainfall patterns, which may lead to more frequent droughts and/or flooding events in coastal areas (Findell and Delworth 2005; Hoerling and Kumar 2003; Manabe and Wetherald 1986). The impact of temperature increase and sea level rise in coastal areas has been examined experimentally (Hazelden and Boorman 1999; Holmer et al. 2002; Laiho 2006; Simas et al. 2001; Weston et al. 2006). In wetlands, it is well known that hydrological shifts can influence plant communities (Forbes and Dunton 2006; McKee et al. 2004) and soil and sediment microbiology and geochemistry (Knorr and Blodau 2009; Knorr et al. 2008). However, the impacts of extreme and shifting climatic conditions are not well understood and the effects of transient droughts on sediment geochemistry and microbial pathways and the consequences of these effects on marsh plant dynamics are poorly constrained.

Spartina alterniflora salt marsh sediments are rich in organic matter due to high plant production and sediment trapping (Adam 1990). Oxygen is typically depleted in the top millimeters and the marsh sediment column is thus largely anoxic (Furukawa et al. 2004). Oxic or suboxic microzones in marsh sediments can be caused by bioturbation (Kostka et al. 2002; Kristensen and Kostka 2005) or via release of oxygen through plant roots (Gribsholt and Kristensen 2002; Holmer et al. 2002). Despite localized or ephemeral

oxygenation of salt marsh sediments, sulfate (SO_4^{2-}) reduction is the dominant pathway of anaerobic carbon oxidation (Howarth and Giblin 1983), though in some cases, iron (Fe(III)) reduction is equally or more important (Hyun et al. 2007; Koretsky et al. 2003; Kostka et al. 2002).

Under drought conditions, a decrease in sediment water content leads to crack formation, which may increase oxygen penetration into soils, promoting aerobic processes. With the onset of oxic conditions, a large fraction of the sediment oxygen consumption is due to re-oxidation of reduced metabolites (Glud 2008; Soetaert et al. 1996), which fuels elemental recycling. For example, Fe(II) oxidation renews the reactive Fe-(hydr)oxide pool, sustaining Fe(III) reduction (Weiss et al. 2004), while the oxidation of reduced sulfur compounds prevents sulfate depletion by high sulfate reduction rates (Moses and Herman 1991). Intermittent oxic conditions further affect organic matter mineralization because aerobic metabolism can break down refractory organic compounds, such as lignin (Canfield 1994), releasing labile organic compounds that are further oxidized via anaerobic metabolic pathways. Such cooperative metabolism of complex polymers is particularly important in salt marsh environments, where a large part of the organic matter is derived from macrophyte vegetation.

Drought has been identified as a factor promoting acute salt marsh vegetation dieback along the U.S. East and Gulf coasts over the last decade (McKee et al. 2004). Marsh dieback could result from drought-derived changes in soil chemistry, such as decrease in pH and increased concentration of toxic metals due to oxidative weathering of metal-sulfides to sulfuric acid and the concomitant release of sulfide-bound trace metals (McKee et al. 2004). Thus far, specific connections between drought, sediment geochemistry, and marsh dieback have escaped documentation. We used sediment flow-through reactors to simulate and evaluate the effects of drought on sediment biogeochemistry and monitor porewater and solid phase geochemical changes during incubation of intact sediment from a Sapelo Island (Georgia) salt marsh. Periods of flooding and drought were simulated by flushing anoxic water or air, respectively, through the sediment. Sediments from a recent dieback area were compared to those from a nearby healthy *S. alterniflora* marsh to assess whether they responded differently to periodic, severe and persistent, or no drought conditions. As pH had been proposed as a potential master variable for the adverse drought-related impact on marsh vegetation, we used both buffered and non-buffered inflow solutions to reveal the effects of fluid buffering on geochemical dynamics.

Materials and methods

Site description and sampling

Experiments were conducted with salt marsh sediment from Marsh Landing (Sapelo Island, Georgia, USA). This site experienced extensive, yet patchy dieback of the dominant vegetation, *S. alterniflora*, in spring 2009. Two locations were sampled, one with healthy vegetation (31.4144, −81.2962) and one with pronounced dieback (31.4150, −81.2954). Eleven intact sediment cores (4.7 cm inner diameter, 15 cm depth), free of macro/meiofauna and vegetation, were collected at each site on May 23 and August 22, 2009 for separate flow-through reactor experiments (see below). Cores were capped hermetically, transported to the laboratory in darkness, and stored overnight at the experimental temperature (25 °C). The following day, sediment from the 2 to 4 cm depth interval from nine replicate cores was collected and quickly transferred into flow-through reactors, where anoxic conditions were imposed. Sediment from the same depth from two additional cores was used for initial solid phase characterization.

Experimental design

For flow-through experiments, a known inflow solution was pumped through sediment reactors at a constant flow rate using a peristaltic pump, and solute concentrations in the outflow water were monitored over time. Polycarbonate reactors (4.7 cm inner diameter × 2 cm high) were enclosed by placing a cap, with inflow/outflow channels at the center and radial grooves to promote uniform distribution of the flowing solutions across the sediment section, at each end. The sediment was enclosed in the reactor housing by a glass fiber filter (0.45 μm GFF), a 0.2 μm nitrocellulose filter, and the reactor caps, which were held together by steel plates tightened with screws; O-ring seals between the sediment compartment and the caps prevented leakage (Pallud et al. 2007).

In both experiments, three different hydrological regimes were applied in triplicate: continuous flooding (control treatment), periodic drought, and severe, persistent drought. All reactors, along with the peristaltic pumps, inflow reservoirs, and tubing, were placed in an anoxic glove bag. Anaerobic, flooded conditions were simulated by perfusing the reactors with anoxic (argon purged) artificial porewater (APW; Table 1). To simulate drought, sterile (0.2 μm filtered) air was flushed through a sub-set of the reactors by removing the inflow tubing from the solution reservoirs, relocating the tubing outside the glove bag, and allowing air to pump through the reactors. The air exiting the reactors was released through tubing that extended from the bag. An unreactive tracer, bromide, was added to the APW to validate the one-dimensional (1-D) flow regime (Pallud et al. 2007) and to evaluate the integrity of 1-D flow following the drought treatments. A flow rate of 1.7 ± 0.1 ml h^{-1} was maintained for both fluid and air flow; this flow rate generated a reactor pore-fluid turnover time of ~ 12 h. The APW composition differed between the two experiments, with the addition of HEPES to provide buffering capacity and lower ammonium levels in the first experiment (May; Table 1).

The buffered experiment ran for 78 days while the non-buffered experiment ran for 64 days. During the initial phase of each experiment, "Stage 1", all reactors were flushed with APW (19 and 10 days in the buffered and non-buffered experiment, respectively).

Table 1 Elemental composition of the artificial porewater (APW) used as inflow solution in the reactors

	Buffered	Non-buffered
NaCl (mM)	300	300
Na_2SO_4 (mM)	20	20
$MgCl_2$ (mM)	15	15
KCl (mM)	5	5
$CaCl_2$ (mM)	2	2
$NaHCO_3$ (mM)	1	1
NH_4^+ (mM)	0.01	1
HPO_4^{2-} (μM)	200	200
Lactate (μM)	250	250
Acetate (μM)	250	250
NaBr (mM)	1.5	1.5
HEPES (mM)	30	–
pH	7.8	7.8

Subsequently, the three hydrological treatments were applied, "Stage 2", extending for 45 days in the buffered experiment and 36 days in the non-buffered experiment. During Stage 2, control reactors continuously received APW, reactors under periodic drought alternated between air-drying and APW-rewetting periods (5–10 day cycles), and reactors under severe drought received a continuous flow of air until they were flooded near the end of the experiment. Stage 2 of the periodic drought treatments ended with a rewetting period in the non-buffered experiment and with an air-drying period in the buffered experiment. At the end of the hydrological manipulation, one of the three replicates was sacrificed for sediment solid phase analyses (these samples are referred to as "Post-Stages 1 + 2"). The other two reactors were again flushed with APW during "Stage 3" (13 and 15 days for the buffered and non-buffered experiment, respectively) to examine the recovery from drought conditions. Upon completion of the experiment, sediment solid phase samples from all remaining reactors were collected for subsequent analysis (these samples are referred to as "Post-Stage 3").

Water exiting the flow-through reactors was sampled every 2 or 3 days for dissolved geochemical analyses during Stages 1 and 3, and during the flooding periods of Stage 2. The input reservoirs were sampled throughout the experiment and no significant deviation from original conditions was observed. Water exiting the reactors was collected into 30 ml syringes connected to the outflow tubing. The flow rate was monitored by measuring the volume collected in the syringes over a known period of time.

Dissolved species analyses

Upon collection, fluid was apportioned into different clean (acid-washed, ultrapure water rinsed, and then combusted at 500 °C for 4 h) vials for various analyses. One ml of sample was used to determine pH using a Thermo® electrode and Thermo® Orion® 4-star pH meter. Five ml of sample was injected into a He purged and crimp-sealed 15 ml headspace vial and acidified with 0.1 ml of concentrated phosphoric acid for subsequent analyses of CH_4 (Joye et al. 2004) and N_2O (Joye and Paerl 1994) concentration. For dissolved inorganic carbon (DIC) analysis, 1 ml of unfiltered sample was injected into a sealed 15 ml glass vial containing 1 ml of concentrated phosphoric

acid to convert DIC to CO_2 and 1 ml of a saturated $CuSO_4$ to eliminate sulfide interference during analysis using a Li-COR® infrared carbon analyzer (LI-820). Ten ml of sample was filtered through a 0.2 µm filter (Target® cellulose, pre-flushed with ultrapure water and air-dried) into a 15 ml polypropylene tube containing 1 ml of 2 N HCl for sulfate (SO_4^{2-}), phosphate (HPO_4^{2-}), bromide (Br^-), dissolved reduced iron and manganese (Fe^{2+}, Mn^{2+}), and trace element (Al^{3+}, Cu^{2+}, Zn^{2+}, Ba^{2+}, Cd^{2+}, and Pb^{2+}) analyses. SO_4^{2-}, HPO_4^{2-} and Br^- were quantified using ion chromatography (Dionex® ICS-2000). Dissolved Fe and Mn concentrations were quantified using atomic absorption spectrophotometry (AA, Perkin-Elmer® AAnalyst 200); speciation between Fe^{2+} and Fe^{3+} was determined using the Ferrozine method (Viollier et al. 2000). Dissolved Mn was assumed to be present as Mn^{2+}. Trace elements were quantified using inductively coupled mass spectrometry (ICP-MS, Perkin-Elmer® Elan 6000) using water samples collected at time zero, at the last time point of Stage 1, and during the final re-flooding period after the treatments (Stage 3).

The remaining porewater sample was filtered (0.2 µm) and split between the following analyses: NO_x ($NO_3^- + NO_2^-$), ammonium (NH_4^+), dissolved organic carbon (DOC), total dissolved nitrogen (TDN), and hydrogen sulfide (HS^-). For NH_4^+, 2 ml of sample were preserved with 0.1 ml of phenol in a 7 ml glass vials and the concentration was quantified using colorimetric techniques (Solorzano 1969). The NO_x concentration was quantified using an Antek® vanadium reduction and nitric oxide chemiluminescent detection system (745 reduction unit and 7050 NO analyzer). DOC and TDN were analyzed on a Shimadzu® total organic carbon analyzer (TOC-V) with a Total nitrogen measurement unit (TNM-1). Dissolved organic nitrogen (TON) was estimated by difference ($TDN - (NH_4^+ + NO_x)$). Samples for HS^- quantification were preserved with 0.5 ml of 20 weight % zinc-acetate and the concentration was determined using colorimetry (Cline 1969).

Sediment solid phase analyses

Solid phase characterization was performed on initial samples (2 cores), at the end of stage 2 (1 reactor per treatment), and at the end of stage 3 (2 reactors per treatment). Each solid phase analysis was performed on 3 subsamples from each reactor to assess cm-scale variability. Sediment sub-samples were frozen under anoxic conditions for subsequent analysis of Fe and Mn oxyhydroxides and exchangeable NH_4^+. For total reduced sulfur (TRS) analysis, sub-samples were preserved in Zn-acetate. A known volume of sediment was dried (80 °C) to determine porosity and bulk density and then it was ground using a mortar and pestle and stored for subsequent analysis of C and N content, and extractions of total P, Fe, and Mn.

Total C (TC) and total N (TN) were determined using high temperature combustion (Thermo Finnigan® Flash 1112 Series elemental analyzer). Total organic carbon (TOC) was determined separately after removal of inorganic carbon by fuming with hydrochloric acid (Hedges and Stern 1984); the carbonate content (TIC) was estimated by difference ($TIC = TC - TOC$). Total P, Fe, and Mn were extracted according to Poulton and Canfield (2005). Concentrations of Fe and Mn in the digestion extracts were quantified using the atomic adsorption spectroscopy (AAS); P concentrations were measured colorimetrically (Murphy and Riley 1962).

Solid phase Fe(III) and Mn(III/IV) oxyhydroxides were sequentially extracted. Adsorbed Fe^{2+} and Mn^{2+} were extracted using buffered ferrozine (Hyacinthe et al. 2006) immediately after reactor disassembly. The concentrations of Fe^{2+} and Mn^{2+} in the ferrozine extract were measured using AAS. Analyses of HPO_4^{2-}, Al^{3+}, Cu^{2+}, Zn^{2+}, Cd^{2+} and Pb^{2+} were also conducted in the ferrozine extracts using ICP-MS. Amorphous and poorly crystallized Fe and Mn minerals (e.g. ferrihydrite) were extracted with ascorbate at pH 7.5 (Hyacinthe and Van Cappellen 2004). Then, well-crystallized oxides (e.g. goethite and hematite) were extracted using sodium dithionite (pH 4.8; Poulton and Canfield 2005). TRS ($H_2S + FeS + FeS_2 + S^0$) was extracted in an acidic Cr^{2+} solution (Fossing and Jorgensen 1989; Ulrich et al. 1997). The acid volatile sulfide (AVS) fraction of TRS ($AVS = FeS + H_2S$) was quantified separately by a simple acid extraction (Morse and Cornwell 1987). Sediment-exchangeable NH_4^+ was extracted with 2N NaCl (Weston et al. 2006) and quantified using standard colorimetric techniques (Solorzano 1969).

Rate calculations

For adsorbed (Fe^{2+}, HPO_4^{2-}, and NH_4^+) and solid phase constituents (Fe(III)-oxides, Mn(IV)-oxides, TIC, TRS, and TP), net rates were calculated for Stages 1 + 2 and Stage 3, respectively, from the difference in concentrations at the start (C_{st}) and the end (C_{end}) of each period (T, in hours):

$$R = (C_{end} - C_{st}) / T \quad (1)$$

For dissolved constituents (DIC, SO_4^{2-}, HS^-, Fe^{2+}, Mn^{2+}, HPO_4^{2-}, and NH_4^+) rates of consumption or production were calculated for each sampling point during wet periods, and net rates over Stages 1 + 2 and Stage 3 were then calculated as:

$$R = \sum \{(C_{out}(t) - C_{in}) \times Q / V \times \Delta t\} / T \quad (2)$$

where Q is the volumetric flow rate, V the volume of the reactor cell, C_{in} the concentration in the inflow and C_{out} the concentration in the reactor outflow. The sum accounts for all time intervals (Δt) in which net production/consumption was detected.

Net rates for organic matter breakdown were estimated as:

$$\sum C_{EST} = SR + FeR + MnR + DNF \quad (3)$$

where $\sum C_{EST}$ is the total anaerobic organic matter mineralization associated with microbial SO_4^{2-} reduction (SR), Fe(III) reduction (FeR), Mn(IV) reduction (MnR) and denitrification (DNF), respectively. Net rates of SR were estimated using Eq. 2 for periods in which sulfate concentrations in the inflow exceeded those in the outflow; FeR and MnR net rates from consumption of total reducible Fe(III)- and Mn(IV)-oxides, respectively; and DNF net rates from NO_3^- consumption following each period of drought (assuming it equivalent to NO_3^- consumption), which applies to Stages 2 and 3 in reactors experiencing drought. Net inorganic carbon production from SR, FeR, MnR and DNF was estimated using ratios of 2, 0.25, 0.5 and 1.125 C produced per SO_4^{2-}, Fe(III), Mn(IV) and NO_3^- consumed, respectively (Canfield et al. 2005).

Sulfide oxidation and nitrification net rates were estimated from the difference between inflow and outflow concentrations (following Eq. 2) during the respective time periods when SO_4^{2-} concentrations in the outflow exceeded those in the input and when NH_4^+ concentrations in the outflow were lower than those in the inflow (assuming that all NH_4^+ consumed was oxidized during drought periods and that NH_4^+ assimilation by bacteria was not important), corrected by the amount of NH_4^+ desorbed during drought relative to control reactors.

Results

Geochemistry

Imposed drought conditions did not significantly affect porewater flow patterns through the reactors (data not shown). No significant differences were observed in dissolved constituents between vegetated and dieback sediments ($p < 0.05$), so the results reported represent the average of the two sediment types. However, significant differences in solid phase constituents were often observed between the two sediment types so those results are reported separately. Strong treatment effects were noted in both the buffered and non-buffered experiments, as described below.

pH

In the buffered experiment control reactors, no significant change in pH over time was noted (7.7 ± 0.1; Fig. 1a). In contrast, drought-impacted reactors exhibited a significant pH decrease (by 0.2 to 0.4 pH units, $p < 0.001$) that recovered gradually after re-flooding. In the non-buffered experiment, the pH of control reactor outflow was stable (6.9 ± 0.1) during the first 20 days, and then increased gradually to 7.8, the pH of the inflow solution (Fig. 1b). The outflow from the periodic and severe drought reactors exhibited significant pH drops (by 0.3 to 0.5 pH units, $p = 0.002$). Though the pH increased during Stage 3 of the non-buffered experiment, even after 2 weeks of flushing, the pH in the drought reactors was lower than that observed in the controls.

Dissolved carbon

Buffer addition affected DIC concentration patterns (Fig. 1c, d). For control reactors, DIC in the reactor outflow was relatively constant (2–3 mM) over the

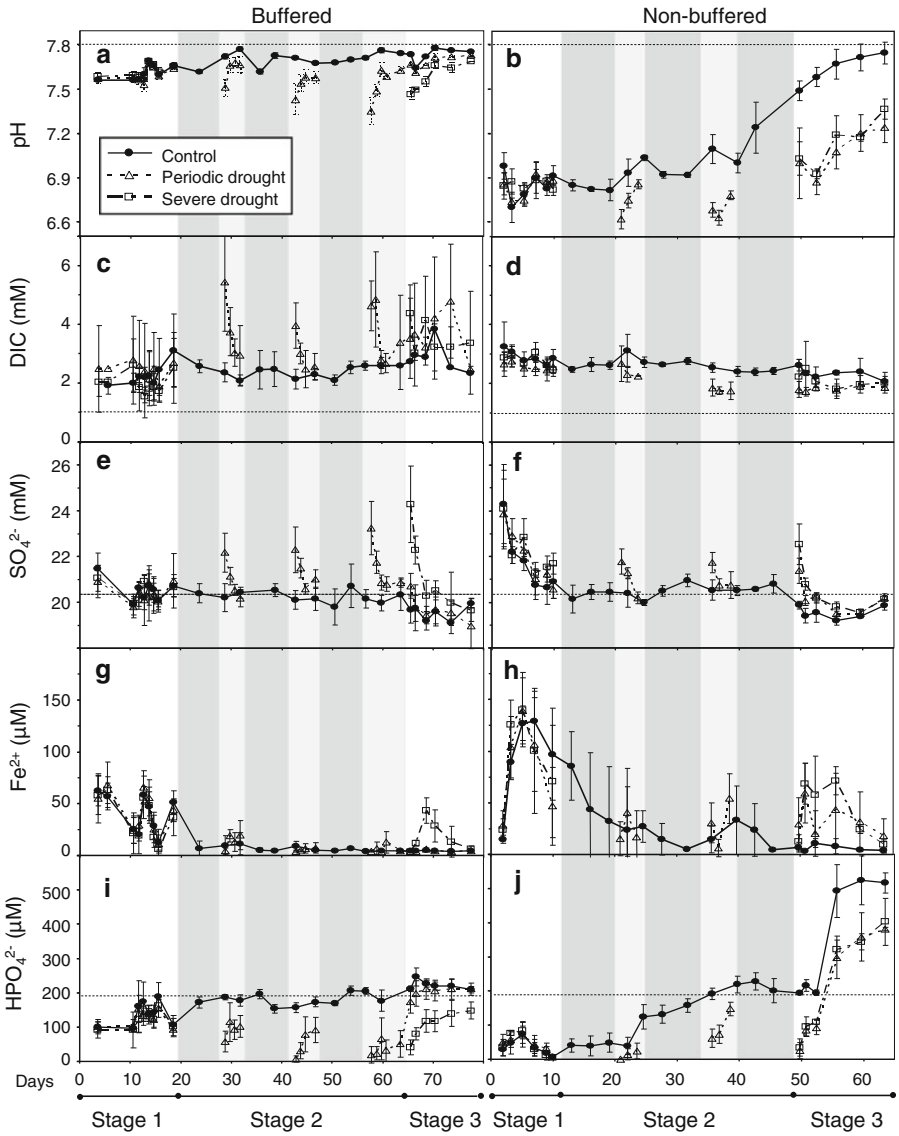

Fig. 1 pH and concentrations of dissolved inorganic carbon (DIC), sulfate, reduced iron, and phosphate, in the flow-through reactor outflowing water in the buffered (*panels on the left*) and non-buffered experiment (*panels on the right*). Data from the vegetated and the dieback sites were averaged. Values are mean ± standard deviation (S.D.); $n = 6$ from day 0 to day 64 (buffered) and to day 46 (non-buffered), and $n = 4$ from then to the end of the experiments. The *gray areas* indicate the periods of drought; the *light gray* zone corresponds to the time periods in which only the severe drought reactors were drying and the periodic drought reactors were flooded. The *horizontal dashed line* indicates the concentration in the inflow solution concentration (0 for Fe^{2+})

course of both experiments. However, after drought periods in the buffered experiment, DIC concentrations increased significantly by a factor of 1.6–2.3 compared to the control. In contrast, in the non-buffered experiment, post-drought DIC concentrations decreased to 70–90 % of the concentration observed in control outflow water. CH_4 concentrations (between 0 and 2 μM; data not shown) were insignificant compared to DIC. No significant differences ($p < 0.05$) in DOC concentrations were observed over time or between treatments (data not shown).

Sulfate and sulfide

Sulfate concentrations in the outflow water exceeded that in the inflow (20.5 mM) during Stage 1 ($p < 0.001$) (Fig. 1e, f). Soon after, SO_4^{2-} concentrations in the control outflow were close to 20.5 mM. SO_4^{2-} concentration increased significantly ($p < 0.05$) in response to drought in both experiments but returned to control levels within 3–4 days of re-flooding. During Stage 3, a significant decrease ($p < 0.05$) in sulfate concentration relative to the inflow concentration was observed consistently. Sulfide concentrations (data not shown) were below detection in the buffered experiment, but reached roughly 60 μM at the end of Stage 3 in the non-buffered experiment.

Iron

During Stage 1 of both experiments, Fe^{2+} in the outflow water of all the reactors exceeded inflow concentrations (Fig. 1g, h), with maxima of 63 ± 6 and 135 ± 7 μM in the buffered and non-buffered experiments, respectively. Fe^{2+} concentrations were significantly higher than controls only in the severe drought treatments during Stage 3 ($p < 0.05$). Dissolved Fe^{2+} concentrations showed substantial variability between reactors, in particular in the non-buffered experiment.

The hydrological regime had distinct impacts on the concentrations of adsorbed Fe^{2+} (Fig. 2). Between the start of the experiment and the end of Stage 2, adsorbed Fe^{2+} concentrations increased significantly ($p < 0.001$) in control treatments in both experiments and with periodic drought in the buffered experiment and dieback sediments of the non-buffered experiment. In contrast, severe drought in vegetated sediments of both experiments and periodic drought in vegetated non-buffered sediments caused significant decreases in adsorbed Fe^{2+} concentrations. During Stage 3, adsorbed Fe^{2+} concentrations either increased or remained at similar levels, with the exemption of control vegetated sediments in the non-buffered experiment, whose concentrations significantly decreased ($p < 0.05$).

Inorganic phosphorus

In the buffered experiment, HPO_4^{2-} concentration in the outflow were comparable to those in the inflow solution (~190 μM) after the Stage 1 (Fig. 1i). Under drought conditions, HPO_4^{2-} concentrations dropped and were significantly lower than in the control, before gradually recovering during re-flooding. In the non-buffered experiment (Fig. 1j), concentrations of HPO_4^{2-} in the outflow were below those of the inflow solution until day 32. During Stage 3, HPO_4^{2-} concentrations generally increased over time, with highest values observed in the control reactors (up to a maximum of 523 μM in the non-buffered experiment).

Drought conditions significantly increased adsorbed P relative to initial concentrations after Stages 1 + 2 ($p < 0.05$, Fig. 2), except for control reactors in the non-buffered experiment. During Stage 3, a general decrease in adsorbed P was observed, though it was only statistically significant in vegetated sediments in the buffered control reactors, and buffered dieback sediments in the periodic drought reactors.

Inorganic nitrogen

Similar patterns for NH_4^+ and NO_x concentrations exiting the reactors were observed in both experiments (Fig. 3a–d). During Stage 2, NH_4^+ in the outflow water of the control reactors closely matched the inflow concentrations, and NO_x concentrations remained below 2 μM. Drought induced a dramatic decrease in NH_4^+, and—with the exception of one drying period—a significant increase in NO_x. Following drought, NH_4^+ returned gradually to the inflow solution concentration; NO_x concentration increased briefly following re-flooding.

Exchangeable NH_4^+ increased significantly ($p < 0.001$) in flooded control reactors of both experiments and periodic drought reactors of the buffered experiment (Fig. 2), reaching comparable maximum levels (~6 μmol gDW^{-1}) in both experiments. In contrast, after severe drought (both experiments) and in the periodic drought reactors in the non-buffered experiment, NH_4^+ concentrations were lower than initial levels. After Stage 3, exchangeable NH_4^+ increased in all the drought-exposed reactors and approached control levels.

Trace metals

Pore water dissolved Mn^{2+}, Ba^{2+}, Cu^{2+}, Zn^{2+} and Al^{3+} concentrations during Stage 3 are presented relative to the concentrations at the end of Stage 1

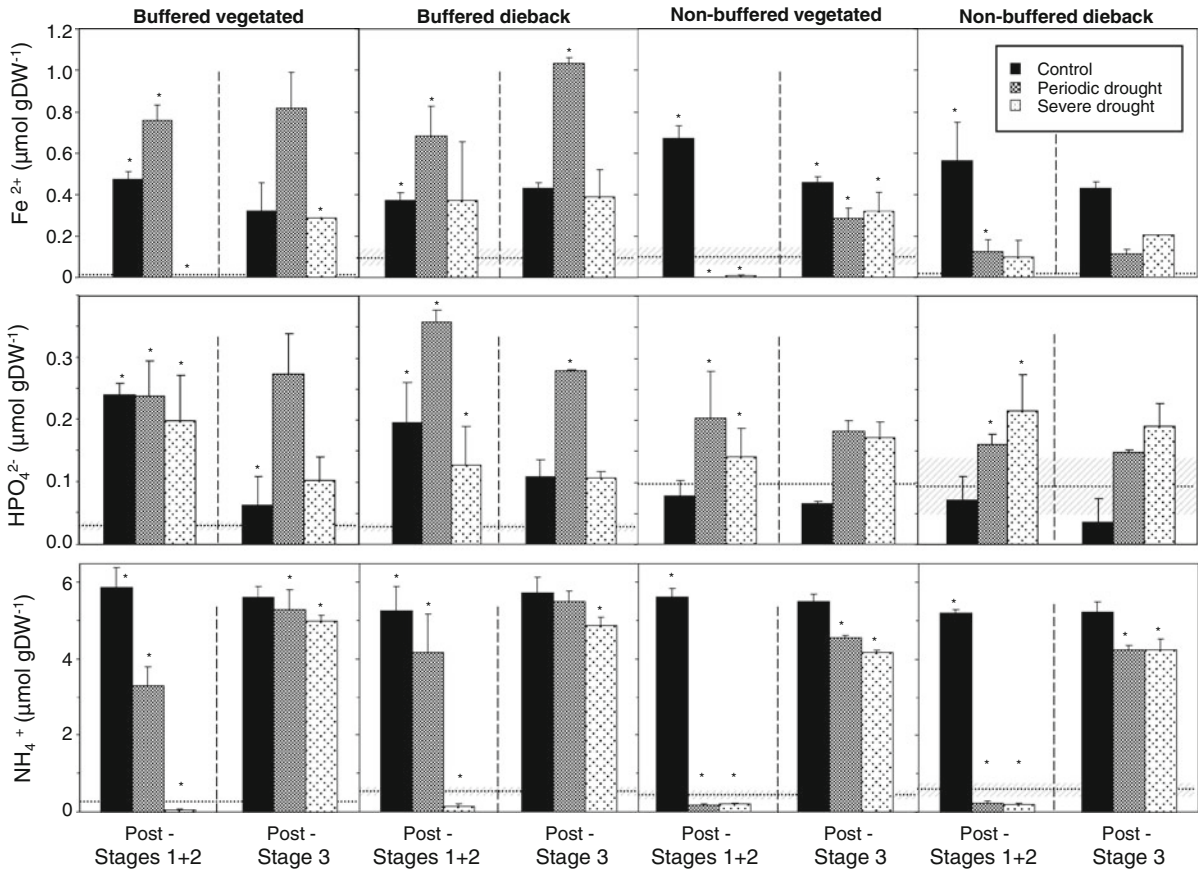

Fig. 2 Concentrations of reduced iron (Fe^{2+}), phosphate (HPO_4^{2-}), and ammonium (NH_4^+) adsorbed to the sediment solid phase of the flow-through reactors. In each row, data are from the buffered (*left two columns*) and the non-buffered experiment (*right two columns*) are presented for the control (*black*), periodic drought (*dark grey*) and severe drought (*dots*) treatments. Average ± standard deviation ($n = 3$) of the initial concentrations are indicated by the *horizontal line* and *diagonally shaded area*. Values 'post-stages 1 + 2' are the average of triplicate measures in one reactor. Values 'post-stage 3' are the average of triplicate measures in two reactors. Significant statistical differences ($p < 0.05$, pair wise) from "initial" to "post-stages 1 + 2", and from "post-stages 1 + 2" to "post-stage 3" concentrations are noted (*asterisk*)

(Fig. 4). Most of these elements exhibited the lowest concentrations in the controls and the highest in the drought reactors, with significant differences ($p < 0.05$) observed only in the buffered experiment. A contrasting pattern was observed for Al^{3+} in the non-buffered experiment, where concentrations were highest in controls at certain time points. Concentrations of $Cd^{2+}$and Pb^{2+} in the pore water were below detection (not shown).

The concentration of the adsorbed trace metals decreased significantly between the start of the non-buffered experiment and the end of Stage 2, except for Cd^{2+} in vegetated control reactors and Zn^{2+} in the drought treatments (Fig. 5). In contrast, in the buffered experiment, adsorbed concentrations in most reactors did not show significant changes during Stages 1 + 2, except for a decrease in most reactors for Mn^{2+} and Pb^{2+}, and Cd^{2+} in the controls, and an increase for Zn^{2+} in vegetated buffered sediments for all reactors. Flooding in Stage 3 in the non-buffered experiment only affected significantly Mn^{2+} concentrations. In the buffered experiment, adsorbed concentrations were significantly lower for Zn^{2+}, Al^{3+} and Cd^{2+} but higher in Mn^{2+} in vegetated sediments of severe drought reactors and significantly higher in Cu^{2+} for vegetated sediments of periodic drought reactors; significant differences were also observed for Pb^{2+} in dieback sediments of drought reactors.

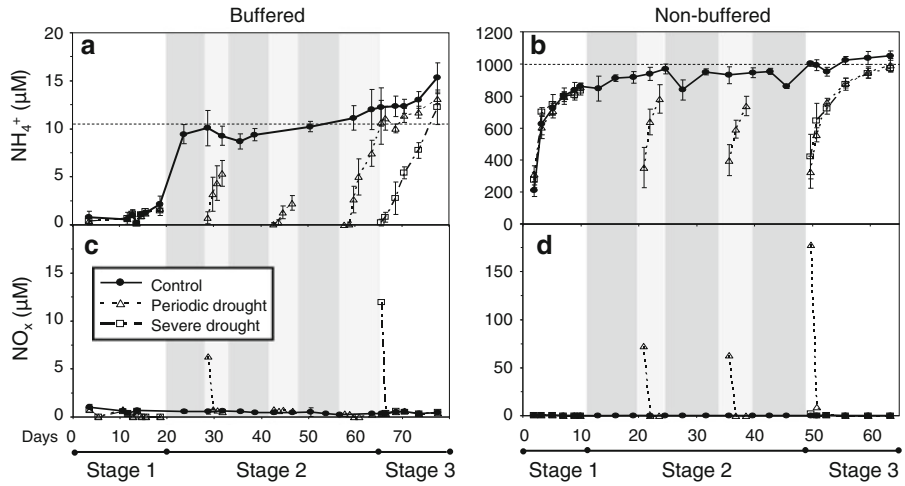

Fig. 3 Concentrations of ammonium (NH_4^+) and nitrate + nitrite (NO_x) in the water exiting the flow-through reactors in the buffered (*panels on the left*) and non-buffered experiment (*panels on the right*). Note the different scales between both experiments for NH_4^+ and NO_x. See caption Fig. 1 for details

Total reducible Fe(III)-oxides

Concentrations of total reducible Fe(III)-oxides (ascorbate- plus dithionite- extracted) after Stages 1 + 2 were significantly lower than initial concentrations ($p < 0.05$), except in vegetated sediments of drought reactors in the buffered experiment and dieback sediments of periodic drought reactor in the non-buffered one (Fig. 6).

Total reducible Mn(IV)-oxides

Reducible Mn(IV)-oxide concentrations decreased significantly between time zero and the end of Stage 2 in control (both sites) and dieback sediments of the periodic drought reactors of the buffered experiment, and in all treatments at the dieback site of the non-buffered experiment (Fig. 6).

Total inorganic carbon

Sediment carbonate content differed significantly between the two collection dates for both vegetated and dieback sites ($p < 0.05$). During Stages 1 and 2 in the buffered experiment, TIC content increased significantly ($p < 0.001$) in all vegetated sediments and in the dieback sediment under drought treatments (Fig. 6). TIC concentrations were often significantly higher in drought reactors than in control reactors. In the non-buffered experiment, TIC concentrations after Stage 2 were not significantly different from the initial values, which were extremely variable. After Stage 3, TIC concentrations increased in control reactors in dieback sediments of the buffered experiment and in vegetated sediments of control and periodic drought reactors in the non-buffered one, but decreased in the non-buffered dieback sediments under periodic drought.

Reduced sulfur

Sediment TRS increased with the continuous flooding in control reactors in both experiments ($p < 0.05$) during Stages 1 + 2, reaching the highest concentrations (76–80 µmol gDW^{-1}) after Stage 3 in the non-buffered experiment (Fig. 6). The periodic drought treatment often generated a larger TRS pool than severe drought, but TRS concentrations never exceeded 40 µmol gDW^{-1}. AVS, which was only above detection in control sediments (both experiments) and in vegetated sediment from the periodic drought treatment of the buffered experiment, representing between 21 and 71 % of the TRS. In the buffered experiment, AVS was only detected after Stage 3.

Total phosphorus

During Stages 1 + 2, total phosphorus (TP) increased significantly from initial concentrations ($p < 0.05$,

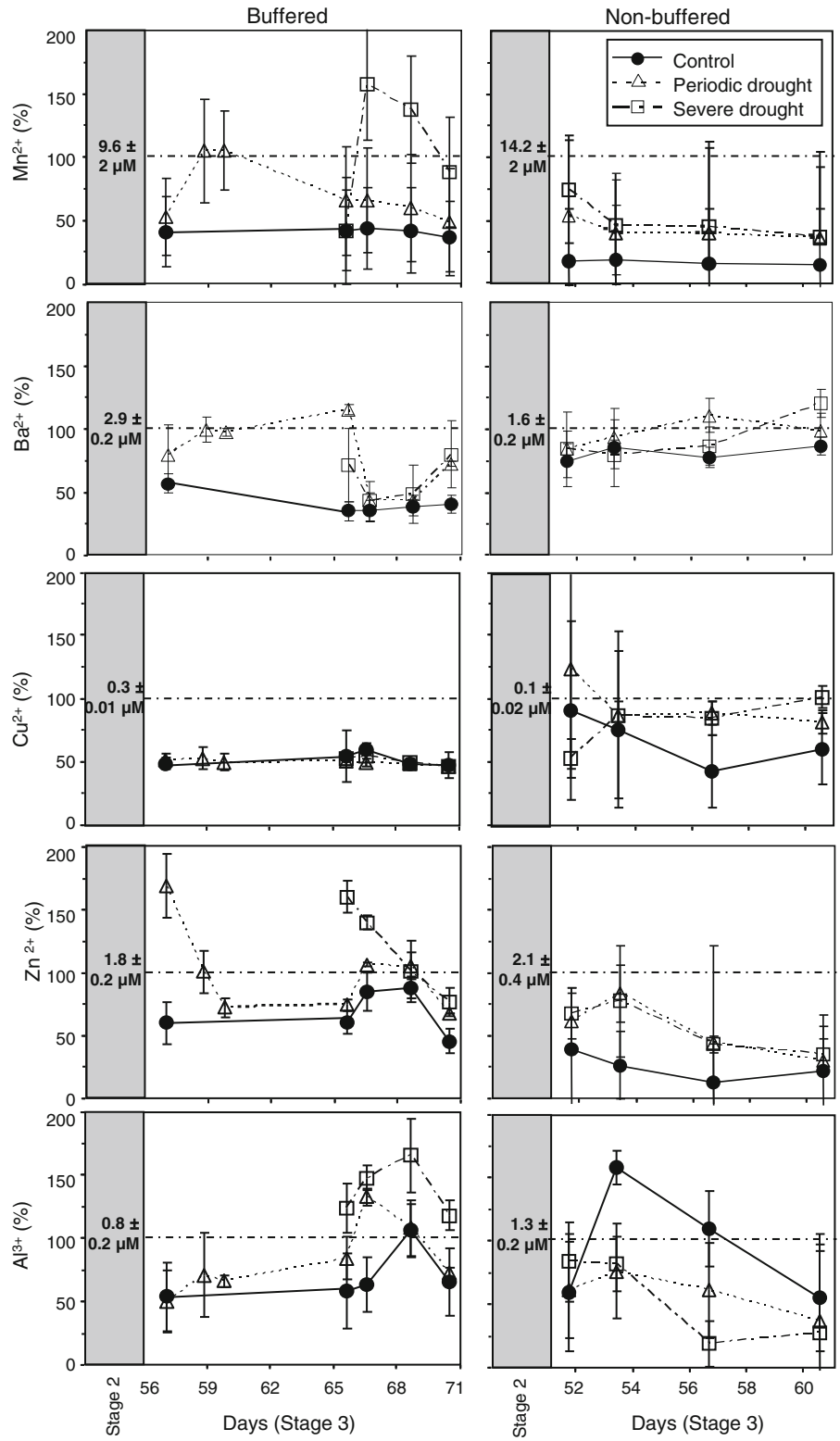

Fig. 4 Percentage of dissolved Mn^{2+}, Ba^{2+}, Cu^{2+}, Zn^{2+}, and Al^{3+} concentrations during Stage 3 relative to the average concentration in each experiment prior to the treatments (i.e. at the end of Stage 1, at day 19 and 10 in the buffered and non-buffered experiment, respectively; $n = 4$)

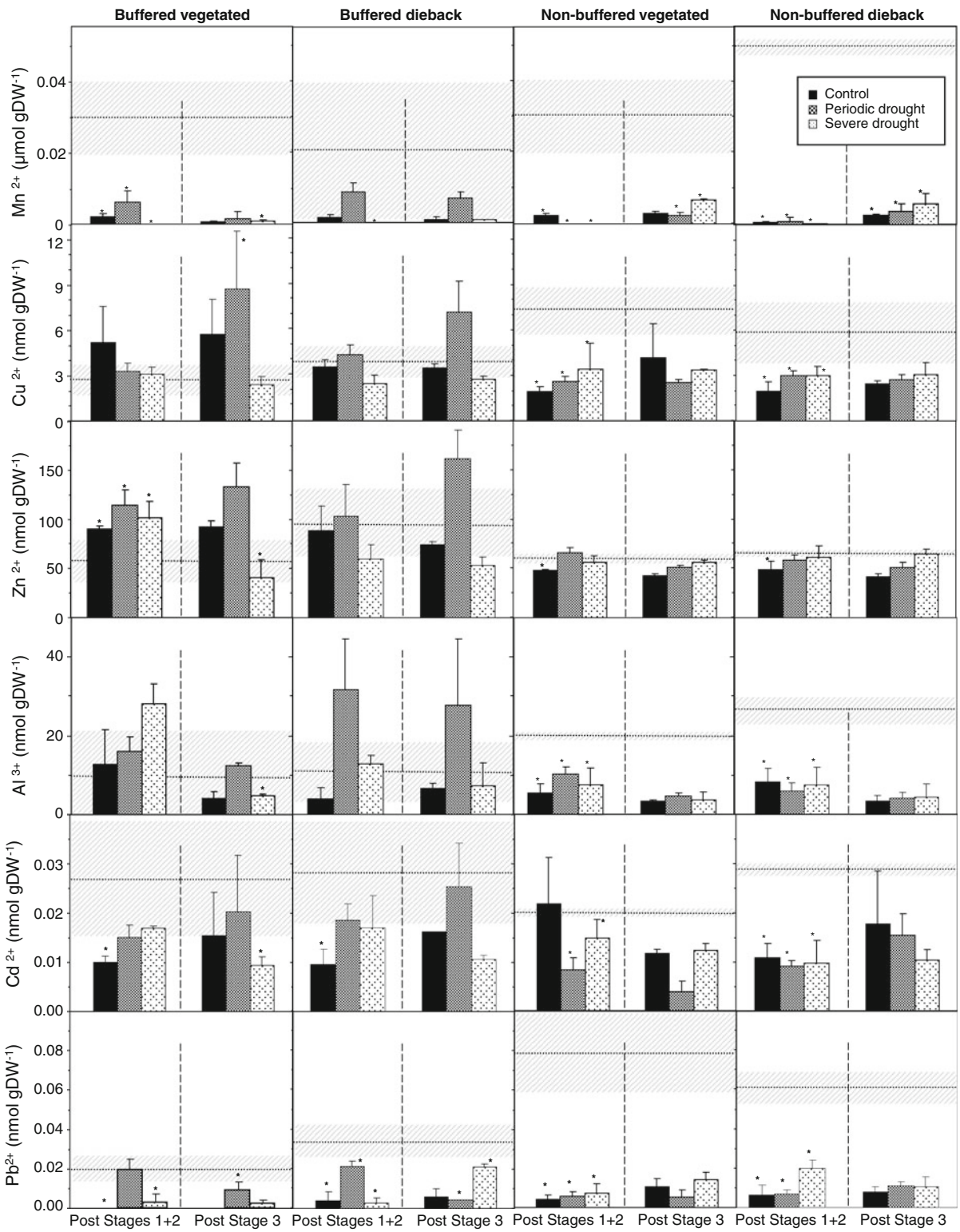

Fig. 5 Concentrations of adsorbed Mn, Cu, Zn, Al, Cd, and Pb in buffered (*left two columns*) and non-buffered experiments (*right two columns*). See caption Fig. 2 for details

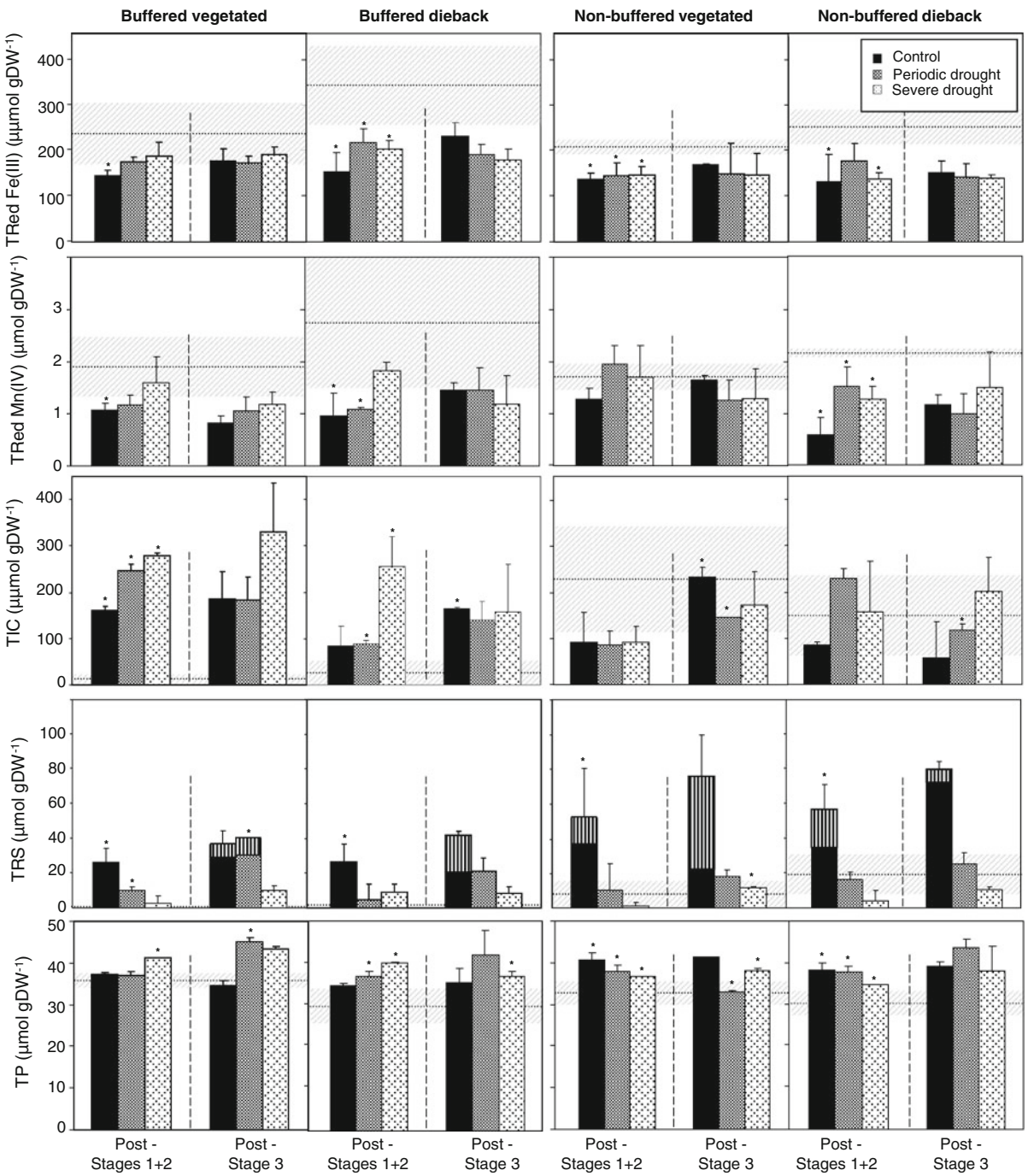

Fig. 6 Concentrations of total reducible (TRed) Fe(III)-oxides, TRed Mn(IV)-oxides, total inorganic carbon (TIC), total reduced sulfur (TRS), and total phosphorus (TP) in the reactor solid phase. *Vertical striped area* represents AVS fraction of TRS. See caption Fig. 2 for details

Fig. 6), except in control reactors (both sites) and vegetated sediments in periodic drought reactors in the buffered experiment. In the non-buffered experiment, the largest increases were observed in control reactors, while in the buffered one, higher concentrations were observed after drought. During Stage 3, significant changes were only detected in periodic drought reactors from vegetated sediments in the buffered

experiment and in dieback sediments in the non-buffered one.

Microbial rates

Estimated anaerobic *C* production ($\sum C_{EST}$), computed as the sum of SO_4^{2-} reduction (SR), Fe(III) reduction (FeR), Mn(IV) reduction (MnR) and denitrification (DNF) (Eq. 3), was compared to carbon produced in terminal metabolism ($\sum C_{MSD}$) measured as the sum of DIC and CH_4 production (Eq. 2) and TIC accumulation (Eq. 1). During Stages 1 + 2 of the buffered experiment, $\sum C_{MSD}$ was consistently higher than $\sum C_{EST}$ in all the reactors (Fig. 7).

SR accounted for the majority of terminal metabolism (an average of 79 and 64 % of $\sum C_{EST}$, in buffered and non-buffered experiments, respectively; Fig. 7), and the SR contribution was usually lower in

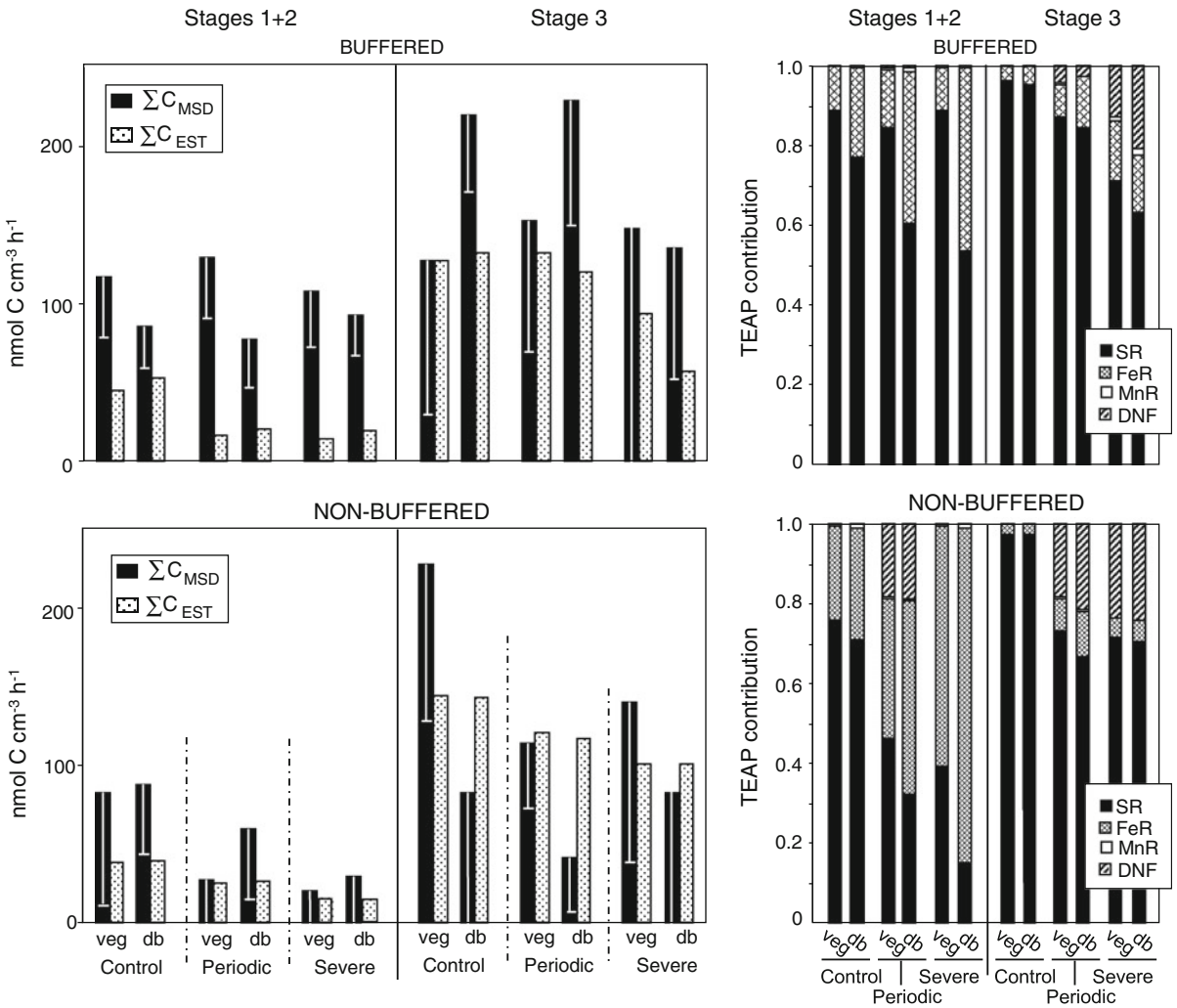

Fig. 7 *Left panels* net rates of anoxic inorganic carbon production ($\sum$C) in buffered (*top panel*) and non-buffered (*bottom panel*) experiments, during Stages 1 + 2 and Stage 3 derived from C measurements ($\sum C_{MSD}$ = DIC + CH_4 + TIC production) and estimated net consumption rates of terminal electron acceptors ($\sum C_{EST}$ = SR + FeR + MnR + DNF), respectively. *Error bars* denote ±1 standard deviation of measured DIC, CH_4 and TIC production rates. *Right panels* estimated contribution of SR, FeR, MnR, and DNF terminal electron accepting processes (TEAP) to total anaerobic organic carbon oxidation in buffered (*top*) and non-buffered (*bottom*) sediments. *veg* and *db* denote vegetated and dieback sites, respectively. SR = SO_4^{2-} reduction, FeR = Fe(III) reduction, MnR = Mn(IV) reduction, and DNF = denitrification. See text for details

drought compared to control reactors. For drought-impacted reactors, the minimum SR contribution (12 %) was observed in Stages 1 + 2 in the non-buffered experiment for dieback sediments under severe drought. SR increased in all the reactors from Stage 1 + 2 to Stage 3 (average net rates were 17 ± 13 and 96 ± 31 nmol C cm^{-3} h^{-1}, respectively), although differences were only significant in non-buffered sediments in control and periodic drought treatments ($p < 0.05$). Nonetheless, drought reactors consistently showed lower average rates than controls (20–40 % lower) during Stages 1 + 2. No differences in net SR rates were observed between vegetated and dieback sediments or between experiments.

The largest contribution of FeR to terminal metabolism in both experiments was observed in drought-influenced reactors, coinciding with low average SR rates. On average, FeR accounted for 25 and 49 % of terminal metabolism in drought reactors during Stages 1 + 2, in buffered and non-buffered experiments, respectively. During Stage 3, the contribution of FeR to metabolism in drought reactors decreased (to 14 and 8 % on average for buffered and non-buffered reactors), but was still larger than in control reactors (3.5 % on average). Variability in FeR rates was high and no significant differences were observed between stages, treatments, experiments, or sites. However, average net rates, which varied between 1 and 15 nmol C cm^{-3} h^{-1}, consistently tended to be higher in non-buffered versus buffered experiment, and in dieback versus vegetated sediments.

DNF contributed to terminal metabolism in sediments that were exposed to drought during the anoxic periods that followed drought (wet periods in Stages 2 and 3). DNF was ephemerally detected (only in 7–15 % of the total time in wet conditions), with net rates up to 320 nmol C cm^{-3} h^{-1}. The net contribution of DNF to terminal metabolism during Stages 1 + 2 was minimal (0.4 %) in periodic drought reactors of the buffered experiment, but up to 17 % in the non-buffered experiment. In the drought reactors during Stage 3, DNF represented an average of 11 and 22 % of total $\sum C_{EST}$ produced in buffered and non-buffered experiments, respectively.

MnR rarely accounted for more than 1 % of organic carbon mineralization; its contribution was higher in dieback periodic drought reactors during Stages 1 + 2 and severe drought reactors during Stage 3 in the buffered experiment. MnR net rates in control and drought reactors varied between 0 and 0.6 nmol C cm^{-3} h^{-1}.

Discussion

Dissimilatory SO_4^{2-} reduction was generally the dominant mode of anaerobic terminal metabolism in both experiments, while Fe reduction played a secondary, and DNF in drought reactors only a tertiary role (Fig. 7); Mn reduction was not significant. The transition from SR and FeR to primarily SR reduction suggests that sediment characteristics changed over time, a trend that was also reflected in changes in pH and P dynamics (Fig. 1), most prominent in the non-buffered experiment. Exposure to oxic conditions associated with drought stimulated oxidation of sulfides, ammonium, and Fe(II) (Figs. 1, 2, 3, and 6) and altered patterns of microbial activity when anoxic conditions were reestablished, increasing the contribution of FeR and DNF to terminal metabolism (Fig. 7). Periodic and severe drought treatments generated similar effects. However, in the buffered experiment the alternation of oxic and anoxic conditions in periodic drought treatments enhanced surface adsorption of multiple geochemical species (Figs. 2, 5). Both the buffered and non-buffered experiment showed similar trends between the three treatment regimes, but the relative contribution of terminal metabolic pathways was more affected under non-buffered conditions.

Major microbial and geochemical processes in the anoxic control reactors

The prevalence of dissimilatory SO_4^{2-} reduction was evidenced by the consumption of SO_4^{2-} and production of sulfide (as H_2S and TRS), while Fe reduction was illustrated by the production of dissolved Fe^{2+}, increases in adsorbed Fe^{2+}, and decreases in Fe(III)-oxide concentration over time (Figs. 1, 2, and 6). Production of dissolved Mn^{2+} (data not shown) and consumption of Mn-oxides (Fig. 6) suggest that Mn(IV) reduction also occurred; however, low concentration of Mn-oxides limited the contribution of dissimilatory MnR to $\sum C_{EST}$ (Fig. 7). Neither methanogenesis (no observed methane production) nor denitrification (no nitrate added to input solution) played a significant role in C mineralization in control

treatments. Net SR, FeR and MnR reduction rates (Fig. 7) combined accounted for 40 to 100 percent of the combined production of DIC, CH_4 and TIC ($=\sum C_{MSD}$). Significant differences between $\sum C_{EST}$ and $\sum C_{MSD}$ occurred in the Stages 1 + 2 of the buffered experiment and were likely due to carbonate precipitation (triggered by the composition of the input solution), consistent with computed oversaturation for both calcite and siderite under the experimental conditions.

The net rates of SR during Stage 3 in control reactors were in average of 130 nmol C cm^{-3} h^{-1} and accounted for 95–97 % of $\sum C_{EST}$ (Fig. 7). During Stages 1 + 2, SR also accounted for the majority of organic matter breakdown (70–90 %), but rates were significantly lower (on the order of 40 nmol C cm^{-3} h^{-1}), suggesting a larger role for FeR. Consistent with the increase of SR rate over time, dissolved HS^- was only detectable during Stage 3 (in non-buffered experiment, data not shown).

Iron reduction was the second most important metabolic pathway, accounting for 17–26 % (Stages 1 + 2) and 3–4 % (Stage 3) of $\sum C_{EST}$ (Fig. 7). The higher FeR rates in control reactors during Stages 1 + 2 versus Stage 3 coincided with more elevated dissolved Fe^{2+} concentrations (Fig. 1). However, production of dissolved plus adsorbed Fe^{2+} represented only 2–6 % of the observed decrease in Fe(III)-oxides. Adding reduced iron sulfide precipitates (estimated from TRS accumulation), FeR rates accounted for 70–100 % of Fe(III)-oxides reduced in Stage 3, and between 20 and 45 % in Stages 1 + 2. The discrepancy during Stages 1 + 2 indicate additional Fe^{2+} sinks. Siderite and vivianite were oversaturated ($\Omega > 1$) consistently, suggesting that Fe^{2+} was also removed via precipitation as phosphate and/or carbonate minerals. From Stages 1 + 2 to Stage 3, net rates of FeR decreased 3–4 and 9–10 fold, in buffered and non-buffered experiments, respectively. While numerous factors can affect the reactivity of iron oxides, our data is consistent with a passivating role of Fe^{2+} adsorption (Fig. 2; Roden and Urrutia 2002; Weston et al. 2006; Zachara et al. 2001). Moreover, during Stage 3 (but not in Stages 1 + 2), the dithionite extracted iron oxide pool no longer decreased over time, suggesting that this pool was no longer bioavailable.

Notable changes in solution composition in the control reactors include the increase of porewater pH over time in the non-buffered experiments. pH affects adsorption dynamics and could have been associated with the changes in dissolved HPO_4^{2-} concentrations over time in the non-buffered experiment (Fig. 1). However, as adsorption accounted only for 6–7 % of dissolved HPO_4^{2-} consumed from the input solution during Stages 1 + 2, dissolved HPO_4^{2-} concentrations were apparently controlled by mineral solubility (Fig. 6), consistent with the findings of Weston et al. (2006). During Stage 3, desorption could account for only 1 % of the observed increase of dissolved HPO_4^{2-} concentrations, which therefore was likely caused by dissolution of P-bound minerals (Hyacinthe and Van Cappellen 2004; Weston et al. 2006).

Drought effects on sediment biogeochemistry and microbial processes

Drought effects were manifest through transient changes in porewater composition after re-establishing flow following periods of imposed drought and by changes in solid phase composition. The contribution of SR to total anoxic organic carbon mineralization ($\sum C_{EST}$) during Stages 1 + 2 was usually lower in drought than in control reactors (reflecting lower SR average rates), and other microbial pathways were more important (Fig. 7). Drought-driven alteration of oxic-anoxic conditions resulted in sulfide oxidation reactions during drought periods, evidenced by peaks in SO_4^{2-} concentration (Fig. 1) and lower TRS concentrations in drought reactors compared to controls (Fig. 6), and the subsequent production of reduced S during anoxic periods. Sulfide oxidation rates during dry periods ranged from 4 to 20 nmol S cm^{-3} h^{-1}.

Fe(III) reduction rates during Stages 1 + 2 did not significantly differ between drought and control reactors, but because of lower SR average rates in drought reactors, FeR contributed more to anoxic mineralization of organic matter in the drought reactors (Fig. 7). The contribution of FeR was particularly enhanced in non-buffered conditions and in dieback sediments, which exhibited larger average values of FeR. In both cases, enhanced FeR coincided with a larger decrease in dithionite-extractable Fe(III)-oxides (73 % in the non-buffered versus 31 % in the buffered experiment; and between 6 and 11 % more in dieback versus vegetated sediments). Additionally, the pH difference between the two experiments may have promoted FeR in non-buffered reactors; at the pH range of the experiments, lower pHs can favor

desorption of Fe^{2+} from the Fe(III)-oxide surfaces (Appelo et al. 2002), thus potentially increase Fe(III) bioavailability (Roden and Urrutia 2002; Roden and Zachara 1996; Weston et al. 2006).

During drought periods, TRS compounds were consumed significantly, presumably also resulting in the oxidation of reduced Fe contained in iron sulfides minerals. However, geochemical evidence for dissolved Fe^{2+} oxidation was not clear (Fig. 1), and Fe(III)-oxide concentrations "post-Stages 1 + 2" were not significantly higher in drought versus control reactors (Fig. 6). The absence of a more clear signature of Fe oxidation in the solid phase is attributed (i) to the presence of both oxidative and reductive processes over the duration of the combined Stages1 + 2, and (ii) the large background and significant variability of Fe-oxides concentrations between reactors, both of which mask drought-induced signatures. Decreases in adsorbed Fe^{2+} concentrations in drought relative to control reactors (Stages 1 + 2, Fig. 2) and increases in dissolved Fe^{2+} concentrations are consistent with the drop of pH observed at re-wetting, given adsorption edges of Fe^{2+} on Fe-oxides reported at pH values between 6.5 and 8.5 (Appelo et al. 2002; Weston et al. 2006).

In strong contrast to the control reactors, nitrification and denitrification were significant processes in drought-impacted reactors. Decreases of dissolved and adsorbed NH_4^+ pools and subsequent peaks in NO_x concentration (Fig. 3) revealed episodic nitrification during oxic conditions in the drought-impacted reactors. Due to different concentrations of NH_4^+ in the inflow solutions, nitrification rates were higher in the non-buffered compared to the buffered experiment. Average ammonium oxidation rates of 1.5–3 nmol N cm^{-3} h^{-1} (buffered) and 9–19 nmol N cm^{-3} h^{-1} (non-buffered conditions) were estimated over the duration of drought periods. NH_4^+ removal exceeded NO_x accumulation following the drought periods, suggesting that denitrifying microbial activity acted as an efficient sink for NO_3^-. Denitrification was corroborated by N_2O detection in reactor outflow water (data not shown) only at the sampling times following drought periods and concurrent with the detection and decrease of NO_x in the outflow water.

The consistent pH decrease observed after all drying periods in both experiments confirms the occurrence of oxidative processes during drought, since nitrification and the re-oxidation of sulfides and metals result in pH decrease (Soetaert et al. 2007). The drop in pH in drought reactors may have promoted the observed increases in adsorbed HPO_4^{2-} (Fig. 2) and decreases in dissolved HPO_4^{2-} concentrations (Fig. 1), as a result of pH-dependent sorption of phosphate onto iron oxides (Gao and Mucci 2001). That the natural sediment buffering capacity without external buffer was comparable to that observed under buffered conditions was unexpected. The pH in the non-buffered experiments dropped to near the first dissociation constant for H_2CO_3. The associated increase in dissolved CO_2 levels may have promoted loss of gaseous CO_2 during drought periods, and qualitatively explain the lack of a DIC pulse upon rewetting in the non-buffered treatments (Fig. 1).

Re-flooding and anoxia after drought conditions

In Stage 3, larger contribution of FeR to total anoxic organic carbon mineralization ($\sum C_{EST}$) in most of the drought reactors reflected a trend to increased FeR rates, in contrast to control reactors, where they tended to decrease. Multiple factors could alter the increase of FeR activity, including differences in Fe-oxide composition (80 vs 60 % of ascorbate-extractable Fe(III)-oxides in drought versus control reactors in non-buffered experiments), or in the extent of Fe^{2+} sorption, passivating Fe(III)-oxide surfaces (Fig. 2; Roden and Urrutia 2002; Roden and Zachara 1996; Weston et al. 2006; see above). However, despite a general increase in FeR rates, the contribution of FeR to total anoxic $\sum C_{EST}$ production decreased in most of the reactors during Stage 3 compared to Stages 1 + 2 (Fig. 7). This is because at the beginning of Stage 3, Fe(III) reducers not only competed with SO_4^{2-} reducers for organic carbon, but also with denitrifying bacteria, which used the NO_3^- produced during oxic periods.

The effect of sediment geochemical alterations induced by drought decreased over time during Stage 3 in drought reactors. This was clearly reflected in porewater constituents, whose concentrations were similar in drought and control reactors by the end of the Stage 3 (Figs. 1, 3). In the solid phase data this pattern was not reflected, although for several parameters the difference between drought and control reactors was smaller after Stage 3 than at the end of Stage 2 (e.g., adsorbed NH_4^+ and TIC). The most persistent effect with drought was observed in adsorbed concentrations of iron, phosphate and trace

metals of the periodic drought reactors in the buffered experiment, suggesting that strong chemical interactions were established by frequent alternation of oxic and anoxic conditions.

Drought effect on trace metal dynamics

Intermittent drought generally resulted in an increase of adsorbed metals under buffered conditions, a pattern not found as consistently under non-buffered or severe drought conditions. The highest adsorbed metal concentrations observed in the periodic drought treatment (Fig. 5) matched the pattern observed for adsorbed Fe^{2+} (Fig. 2). Adsorbed Fe^{2+} concentration correlated with concentrations of adsorbed Al^{3+}, Cu^{2+}, and Zn^{2+} ($p < 0.05$) in both experiments and with adsorbed Mn^{2+} in the non-buffered experiment. This correspondence with Fe suggests that these ions were affected by similar processes, including reductive dissolution of iron oxides and the concurrent release of sorbed or co-precipitated metals (e.g., Al^{3+} can substitute isomorphically for Fe^{3+} in Fe(III)-oxide minerals (Haese et al. 2000) and Zn^{2+} is generally adsorbed to Fe-oxides (Bostick et al. 2001)) or precipitation and subsequent re-oxidation—in the drought reactors—of metal-sulfides (Du Laing et al. 2008; Morse and Luther 1999).

Trace metal concentrations in the outflow water of control reactors dropped over the duration of the experiment, in particular under buffered conditions (Fig. 4). Levels observed following drought were typically higher in buffered conditions, although a similar trend was observed in the non-buffered experiment. While enhanced mobilization at lower pH in the non-buffered experiment may have contributed to these observations, the pH range in the reactor experiments was likely too high to cause a significant impact (Bradl 2004; Farley et al. 1985), and in the absence of direct evidence we speculate that other factors such as transformation of sorbent minerals or co-precipitates may be more relevant.

Conclusions

Drought and the onset of transient oxic conditions resulted in a significant alteration of sediment geochemistry and microbial pathways. Drought promoted oxidation of dissolved metabolites, lowered sediment pH, favored Fe(III) versus SO_4^{2-} reduction, induced nitrifying and subsequently denitrifying microbial activity, and increased metal availability. Concentrations of dissolved and adsorbed metals in drought reactors often exceeded those in constantly flooded anoxic sediments. The drought effect on dissolved trace metals concentrations was transient and not significant in non-buffered conditions, but the adsorbed metal concentrations remained elevated after the reestablishment of anoxia, which may affect the bioavailability of metals following small changes in pH or Eh. Sediments from vegetated and dieback areas generally showed similar geochemical patterns and were similarly affected by the hydrological treatments, indicating that the pre-existing conditions of both areas did not alter the effects caused by drought. Our results suggest that the geochemical changes induced by drought could affect the release of metals like Zn^{2+} or Al^{3+} that can be toxic for plant growth, while drought-induced pH alterations alone may not be sufficient to cause marsh dieback. Further research on trace metals dynamics in fluctuating oxic/anoxic environments is warranted. These data illustrate that short-term (<monthly) fluctuations in oxic-anoxic conditions, driven by transitory drought, cause significant changes in salt marsh sediment microbial biogeochemistry. Longer periods of drought promoted by increased global temperatures, or longer sequences of fluctuation between oxic and anoxic conditions, may increase the intensity of changes predicted from the patters observed in this study. These changes likely generate a cascade through the ecosystem, with potentially negative impacts on macrophyte dynamics, and therefore the whole salt marsh ecosystem.

Acknowledgments This publication was supported by the Georgia Sea Grant Program of the National Sea Grant College, NOAA (NOAA grants NA06RG0029-R/WQ11 and R/WQ12A to SBJ) and by the National Science Foundation funded Georgia Coastal Ecosystems Long Term Ecological Research program (OCE 99-82133 and OCE 06-20959). The authors thank our Kim Hunter for scientific discussions and support in the laboratory; Christelle Hyacinthe and Laura Potter for help in the laboratory; and Daniel Saucedo for help in the field.

References

Adam P (1990) Saltmarsh ecology. Cambridge University Press, Cambridge

Appelo CAJ, Van der Weiden MJJ, Tournassat C, Charlet L (2002) Surface complexation of ferrous iron and carbonate

on ferrihydrite and the mobilization of arsenic. Environ Sci Technol 36(14):3096–3103

Bostick BC, Hansel CM, La Force MJ, Fendorf S (2001) Seasonal fluctuations in zinc speciation within a contaminated wetland. Environ Sci Technol 35(19):3823–3829

Bradl HB (2004) Adsorption of heavy metal ions on soils and soils constituents. J Colloid Interface Sci 277(1):1–18

Canfield DE (1994) Factors influencing organic carbon preservation in marine sediments. Chem Geol 114(3–4):315–329

Canfield DE, Thamdrup B, Kristensen E (2005) Aquatic geomicrobiology. Elsevier Academic Press, California

Cline JD (1969) Spectrophotometric determination of hydrogen sulfide in natural waters. Limnol Oceanogr 14(3):454–458

Du Laing G, De Meyer B, Meers E, Lesage E, Van de Moortel A, Tack FMG, Verloo MG (2008) Metal accumulation in intertidal marshes: role of sulphide precipitation. Wetlands 28(3):735–746

Farley KJ, Dzombak DA, Morel FMM (1985) A surface precipitation model for the sorption of cations on metal-oxides. J Colloid Interface Sci 106(1):226–242

Findell KL, Delworth TL (2005) A modeling study of dynamic and thermodynamic mechanisms for summer drying in response to global warming. Geophys Res Lett 32(16)

Forbes MG, Dunton KH (2006) Response of a subtropical estuarine marsh to local climatic change in the southwestern Gulf of Mexico. Estuaries Coasts 29(6B):1242–1254

Fossing H, Jorgensen BB (1989) Measurement of bacterial sulfate reduction in sediments. Evaluation of a single-step chromium reduction method. Biogeochemistry 8(3):205–222

Furukawa Y, Smith AC, Kostka JE, Watkins J, Alexander CR (2004) Quantification of macrobenthic effects on diagenesis using a multicomponent inverse model in salt marsh sediments. Limnol Oceanogr 49(6):2058–2072

Gao Y, Mucci A (2001) Acid base reactions, phosphate and arsenate complexation, and their competitive adsorption at the surface of goethite in 0.7 M NaCl solution. Geochim Cosmochim Acta 65(14):2361–2378

Glud RN (2008) Oxygen dynamics of marine sediments. Marine Biol Res 4(4):243–289

Gribsholt B, Kristensen E (2002) Effects of bioturbation and plant roots on salt marsh biogeochemistry: a mesocosm study. Marine Ecol Prog Ser 241:71–87

Haese RR, Schramm J, van der Loeff MMR, Schulz HD (2000) A comparative study of iron and manganese diagenesis in continental slope and deep sea basin sediments off Uruguay (SW Atlantic). Int J Earth Sci 88(4):619–629

Hazelden J, Boorman LA (1999) The role of soil and vegetation processes in the control of organic and mineral fluxes in some western European salt marshes. J Coastal Res 15(1):15–31

Hedges JI, Stern JH (1984) Carbon and nitrogen determinations of carbonate-containing solids. Limnol Oceanogr 29(3):657–663

Hoerling M, Kumar A (2003) The perfect ocean for drought. Science 299(5607):691–694

Holmer M, Gribsholt B, Kristensen E (2002) Effects of sea level rise on growth of *Spartina anglica* and oxygen dynamics in rhizosphere and salt marsh sediments. Marine Ecol-Prog Ser 225:197–204

Howarth RW, Giblin A (1983) Sulfate reduction in the salt marshes at Sapelo Island, Georgia. Limnol Oceanogr 28(1):70–82

Hyacinthe C, Van Cappellen P (2004) An authigenic iron phosphate phase in estuarine sediments: composition, formation and chemical reactivity. Mar Chem 91(1–4):227–251

Hyacinthe C, Bonneville S, Van Cappellen P (2006) Reactive Fe(III) in sediments: chemical versus microbial extractions. Geochim Cosmochim Acta 70(16):4166–4180

Hyun JH, Smith AC, Kostka JE (2007) Relative contributions of sulfate- and Fe(III) reduction to organic matter mineralization and process controls in contrasting habitats of the Georgia saltmarsh. Appl Geochem 22(12):2637–2651

Joye SB, Paerl HW (1994) Nitrogen cycling in microbial mats. Rates and patterns of denitrification and nitrogen-fixation. Mar Biol 119(2):285–295

Joye SB, Boetius A, Orcutt BN, Montoya JP, Schulz HN, Erickson MJ, Lugo SK (2004) The anaerobic oxidation of methane and sulfate reduction in sediments from Gulf of Mexico cold seeps. Chem Geol 205(3–4):219–238

Knorr KH, Blodau C (2009) Impact of experimental drought and rewetting on redox transformations and methanogenesis in mesocosms of a northern fen soil. Soil Biol Biochem 41(6):1187–1198

Knorr KH, Oosterwoud MR, Blodau C (2008) Experimental drought alters rates of soil respiration and methanogenesis but not carbon exchange in soil of a temperate fen. Soil Biol Biochem 40(7):1781–1791

Koretsky CM, Moore CM, Lowe KL, Meile C, DiChristina TJ, Van Cappellen P (2003) Seasonal oscillation of microbial iron and sulfate reduction in saltmarsh sediments (Sapelo Island, GA, USA). Biogeochemistry 64(2):179–203

Kostka JE, Gribsholt B, Petrie E, Dalton D, Skelton H, Kristensen E (2002) The rates and pathways of carbon oxidation in bioturbated saltmarsh sediments. Limnol Oceanogr 47(1):230–240

Kristensen E, Kostka JE (2005) Macrofaunal burrows and irrigation in marine sediment: microbiological and biogeochemical interactions. Interact Between Macro Microorg Mar Sediments 60:125–157

Laiho R (2006) Decomposition in peatlands: reconciling seemingly contrasting results on the impacts of lowered water levels. Soil Biol Biochem 38(8):2011–2024

Manabe S, Wetherald RT (1986) Reduction in summer soil wetness induced by an increase in atmospheric carbon-dioxide. Science 232(4750):626–628

McKee KL, Mendelssohn IA, Materne MD (2004) Acute salt marsh dieback in the Mississippi River deltaic plain: A drought-induced phenomenon? Glob Ecol Biogeogr 13(1):65–73

Morse JW, Cornwell JC (1987) Analysis and distribution of iron sulfide minerals in recent anoxic marine-sediments. Mar Chem 22(1):55–69

Morse JW, Luther GW (1999) Chemical influences on trace metal-sulfide interactions in anoxic sediments. Geochim Cosmochim Acta 63(19–20):3373–3378

Moses CO, Herman JS (1991) Pyrite oxidation at circumneutral pH. Geochim Cosmochim Acta 55(2):471–482

Murphy J, Riley JP (1962) A modified single solution method for determination of phosphate in natural waters. Anal Chim Acta 26(1):31–36

Pallud C, Meile C, Laverman AM, Abell J, Van Cappellen P (2007) The use of flow-through sediment reactors in biogeochemical kinetics: methodology and examples of applications. Mar Chem 106(1–2):256–271

Poulton SW, Canfield DE (2005) Development of a sequential extraction procedure for iron: implications for iron partitioning in continentally derived particulates. Chem Geol 214(3–4):209–221

Roden EE, Urrutia MM (2002) Influence of biogenic Fe(II) on bacterial crystalline Fe(III) oxide reduction. Geomicrobiol J 19(2):209–251

Roden EE, Zachara JM (1996) Microbial reduction of crystalline iron(III) oxides: influence of oxide surface area and potential for cell growth. Environ Sci Technol 30(5):1618–1628

Simas T, Nunes JP, Ferreira JG (2001) Effects of global climate change on coastal salt marshes. Ecol Model 139(1):1–15

Soetaert K, Herman PMJ, Middelburg JJ (1996) Dynamic response of deep-sea sediments to seasonal variations: a model. Limnol Oceanogr 41(8):1651–1668

Soetaert K, Hofmann AF, Middelburg JJ, Meysman FJR, Greenwood J (2007) The effect of biogeochemical processes on pH. Mar Chem 105(1–2):30–51

Solorzano L (1969) Determination of ammonia in natural waters by phenolhypochlorite method. Limnol Oceanogr 14(5): 799–801

Ulrich GA, Krumholz LR, Suflita JM (1997) A rapid and simple method for estimating sulfate reduction activity and quantifying inorganic sulfides. Appl Environ Microbiol 63(4):1627–1630

Viollier E, Inglett PW, Hunter K, Roychoudhury AN, Van Cappellen P (2000) The ferrozine method revisited: Fe(II)/Fe(III) determination in natural waters. Appl Geochem 15(6):785–790

Weiss JV, Emerson D, Megonigal JP (2004) Geochemical control of microbial Fe(III) reduction potential in wetlands: comparison of the rhizosphere to non-rhizosphere soil. FEMS Microbiol Ecol 48(1):89–100

Weston NB, Dixon RE, Joye SB (2006) Ramifications of increased salinity in tidal freshwater sediments: Geochemistry and microbial pathways of organic matter mineralization. J Geophys Res Biogeosciences 111(G1)

Zachara JM, Fredrickson JK, Smith SC, Gassman PL (2001) Solubilization of Fe(III) oxide-bound trace metals by a dissimilatory Fe(III) reducing bacterium. Geochim Cosmochim Acta 65(1):75–93